OPEN JOURNAL SYSTEMS

Available on line at Directory of Open Access Journals

Journal of Hyperspectral Remote Sensing v.6, n.6 (2016) 283-294
DOI: 10.5935/2237-2202.20160028

Journal of Hyperspectral Remote Sensing
www.ufpe.br/jhrs

Study of biophysical parameters using remote sensing techniques to Quixeré-CE region.

Camilla K. Borges[*], Raimundo M. de Medeiros[*], Roberta E. P. Ribeiro[*], Élder G. dos Santos[*], Rayonil G. Carneiro[**], Carlos A. C. dos Santos[*]

[*] Unidade de Ciências Atmosféricas – UACA da Universidade Federal de Campina Grande – UFCG, Campina Grande – PB, Brasil. camillakassar@gmail.com (Corresponding author)
[**] Instituto Nacional de Pesquisas Espaciais - INPE, Cachoeira Paulista – SP, Brasil.

Received 21 May 2016; accepted 09 June 2016

Abstract

This work aims to analyze the behavior and the spatial variability of energy fluxes, albedo, surface temperature and vegetation index (NDVI) through the SEBAL algorithm, used in remote sensing for different surfaces in the region of Quixeré-EC. It was used TM- Landsat 5 satellite images for the dates October 24, 2005 and August 8, 2006, where the SEBAL algorithm was applied to calculate the fluxes of H, LE, Rn, G, and the surface albedo. From the clippings of a coverage area of banana orchard, savanna and bare soil, in order to check the H + LE and Rn-G components of energy balance. Correlations greater than 0.99 was observed between the components of energy balance H + LE and Rn-G, the relationship between surface albedo and radiation balance in the orchard area showed higher correlations to 0.88, the area comprised by savanna, for the day 297 showed no good correlation between variables, approximately 69% of unexplained variation in day 220 was about 0.88 correlation between the variables, this fact is associated homogeneous characteristics of the area that presented an increase of moisture available in relation to day 297.

Keywords: energy flows, albedo, SEBAL.

1. Introduction

Climate change caused by human action, has brought the need for modeling of environmental parameters of the surface and atmosphere, to learn more about the use of transformation processes and occupation (Bezerra et al., 2014).

With the improvement of the techniques applied in remote sensing for monitoring several meteorological and environmental phenomena, in order to help the weather forecast at, estimating water needs of a culture, crop and climate change, etc. Fact that makes it a valuable tool to contribute to the management of natural resources (Bezerra et al., 2011; Gomez et al., 2011; Cunha et al., 2012; Bezerra et al., 2014).

Some locations, such as Brazil, have lack of meteorological and micrometeorological timely information, making it difficult to obtain these variables. Then, the application of remote sensing techniques make it possible to analyze the spatial variability, making it advantageous technical and budgetary the point of view (Santos, 2009; Borges, 2013).

In this sense, SEBAL (Surface Energy Balance Algorithm for Land) allows the estimation of energy flows that occur in the Earth's surface interface with the atmosphere from the data obtained through remote sensing. Latent heat flow is determined as a residue of the energy balance, the net radiation, heat flow in soil

and sensitive heat flow must be estimated for the model processing steps (Lima et al., 2013).

In this work we were processed satellite images Landsat 5-TM, from Quixeré-EC region, with an interest in farm Frutacor to study the behavior and spatial variability of energy flows, albedo, surface temperature and vegetation index, NDVI in different surfaces.

2. Materials and Methods

2.1 Description of the study area

The study area is located in Frutacor farm (coordinates: 5º08'44 "S, 38º05'53" W), in the municipality of Quixeré-CE (Figure 1), in the microregion of the Lower River Jaguaribe, with an average elevation of 147 m and approximate area 250 ha of banana cultivation Pacovan (Musa sp.). The site presents hot and dry semi-arid climate, BSh type, according to the classification of Koppen-Geiger (Sampaio et al., 2011), with an average annual temperature of 28.5 ° C. The average annual rainfall of 772 mm in a 25-year period (1981-2006), Figure 2 (Santos, 2009; Borges, 2013).

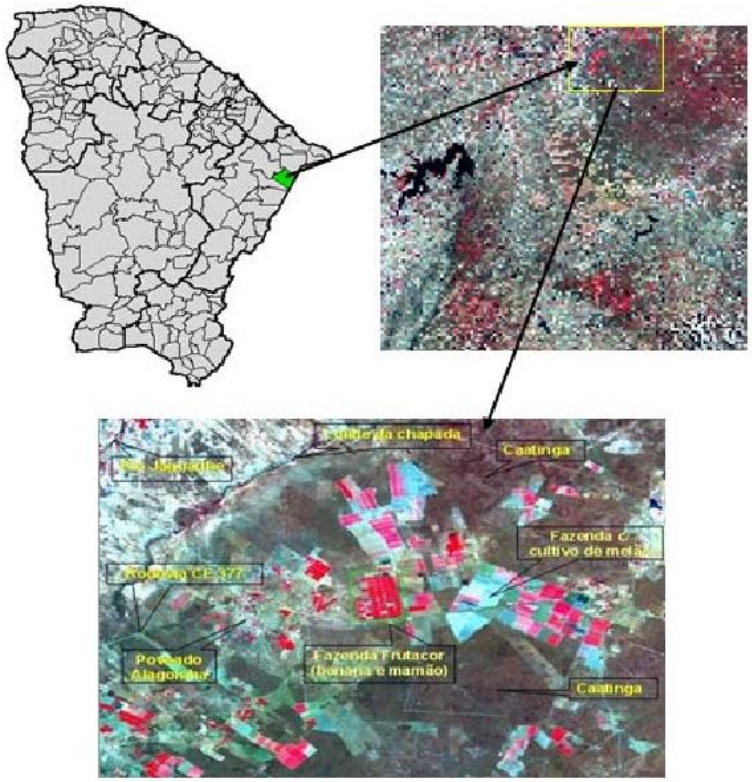

Figura 1 - Highlighting the Quixeré – CE city and image of Landsat 5 - TM, with Frutacor farm location and areas of savanna (Caatinga). Source: Dantas et al. (2010).

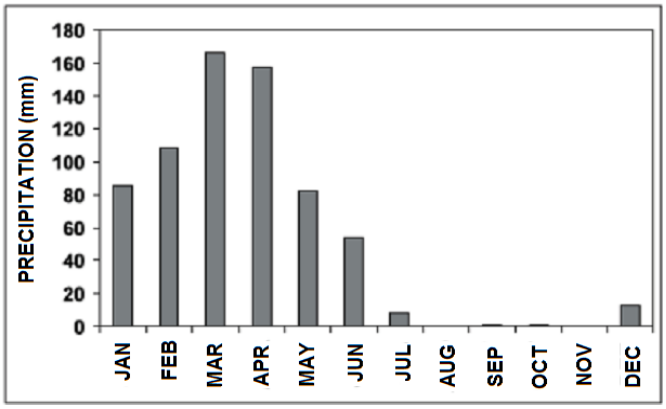

Figura 1 - Distribution of rainfall monthly average from 1981 to 2006. Source: Santos e Silva (2008).

2.2 Radiation balance of processing steps (Rn) and SEBAL.

To calculate the radiation balance at the surface that were followed by some steps described below (Figure 3).

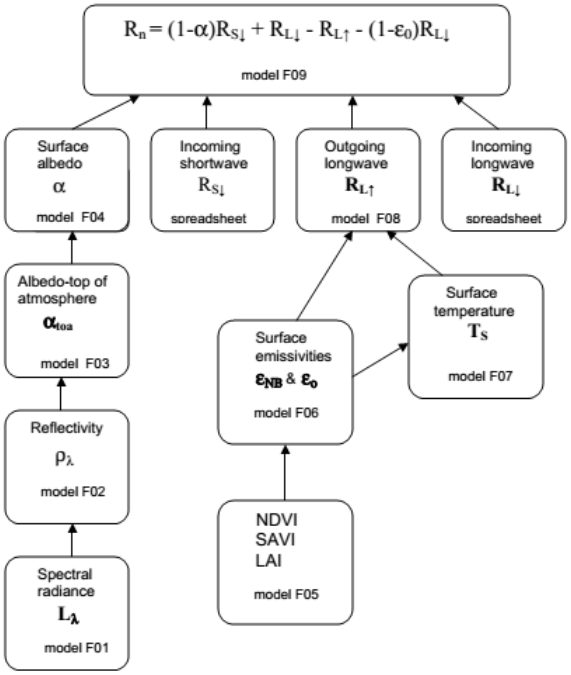

Figura 3 - Calculation of surface radiation balance Source: Allen et al. (2002).

It begins by calculating the spectral radiance or radiometric calibration, given by the following expression ($L_{\lambda i}$):

$$L_{\lambda i} = a_i + \frac{b_i - a_i}{255} ND \quad (Wm^{-2}sr^{-1}\mu m^{-1})$$

where *a* and *b* are the minimum and maximum spectral irradiance; *ND* is the pixel intensity (digital number - integer from 0 to 255) and *i* corresponds to bands (1, 2, ..., 7) of Landsat 5 - TM.

The planetary reflectance of each band, which is defined as the ratio of the reflected radiation flux, and the incident radiation flux, calculated by the following equation (Allen, 2002):

$$\rho_{\lambda i} = \frac{\pi . L_{\lambda i}}{k_{\lambda i} . \cos Z . d_r}$$

where $L_{\lambda i}$ is the spectral radiance of each band $k_{\lambda i}$ is the spectral solar irradiance in each band at the top of the atmosphere, Z is the solar zenith angle and d_r is the inverse square of relative distance Earth-Sun (in astronomical unit - AU) given by:

$$d_r = 1 + 0{,}033 \cos\left(DJ \frac{2\pi}{365} \right)$$

DJ is the Julian day and the cosine function argument given in radians. The solar zenith angle was obtained by the date of the acquired images, which are: December 4, 2000 (JD = 338), Z = 31.28°; October 4, 2001 (JD = 277), Z = 30.03°.

For the computation of the Planetary Albedo (α_{toa}) was used a linear combination of the planetary reflectance obtained in the previous step, valid for a clear day (Allen, 2002):

$$\alpha_{toa} = \sum (\rho_{\lambda i} . \omega_{\lambda i})$$

where $\rho_{\lambda i}$ is the reflectance planetary e $\omega_{\lambda i}$ is a coefficient for each band, presented in Table 1.

Table 1 – Coefficients ω_λ for reflective bands of Landsat 5 - TM.

Bands	**1**	**2**	**3**	**4**	**5**	**6**	**7**
Landsat 5	0,293	0,274	0,233	0,157	0,033	–	0,011

To calculate the Surface Albedo it was used the correction of the planetary albedo for atmospheric transmissivity (Allen, 2002):

$$\alpha = \frac{\alpha_{toa} - \alpha_p}{\tau_{sw}^2}$$

α_p is reflected solar radiation to the satellite ranging between 0.025 and 0.04, but for the SEBAL model is recommended to use the value of 0.03, based on Bastiaanssen (2000), and τ_{sw} is the atmospheric transmittance defined as the fraction of incident radiation transmitted through the atmosphere by the effects of absorption and reflection, for clear sky conditions (Allen, 2002):

$$\tau_{sw} = 0{,}75 + 2.10^{-5} z$$

The Normalized Difference Vegetation Index (NDVI) is given in terms of the bands near infrared (ρ_4) and red (ρ_3) (Allen, 2002).

$$NDVI = \frac{\rho_4 - \rho_3}{\rho_4 + \rho_3}$$

The NDVI is an indicator of the vigor of the vegetation and the amount of green vegetation, ranging from -1 to +1.

To calculate the Soil Adjusted Vegetation Index (SAVI) that is used to mitigate the effects of the "background" of the soil, with the following expression (Allen, 2002):

$$SAVI = \frac{(1+L)(\rho_4 - \rho_3)}{(L + \rho_4 + \rho_3)}$$

, with the constant L=0,5.

The Leaf Area Index (LAI) is an indicator of biomass and enables to estimate the canopy resistance, computed by the following equation (Allen, 2002):

$$LAI = -\frac{\ln\left(\frac{0{,}69 - SAVI}{0{,}59}\right)}{0{,}91}$$

The emissivity of the thermal band (ε_{NB}) and broadband (ε_0) - long wave emitted by the surface. If the NDVI > 0 and the LAI < 3 the following equations are applied:

$$\varepsilon_{NB} = 0{,}97 + 0{,}00331 IAF$$

$$\varepsilon_0 = 0{,}95 + 0{,}01 IAF$$

but if the $IAF \geq 3$, then $\varepsilon_{NB} = \varepsilon_0 = 0{,}98$. In case of water bodies, NDVI < 0 for $\varepsilon_{NB} = 0{,}99$ and $\varepsilon_{0} = 0{,}985$ (Allen et al., 2002).

Determine the surface temperature given by the expression:

$$T_s = \frac{K_2}{\ln\left(\frac{\varepsilon_{NB} K_1}{L_{\lambda,6}} + 1\right)}$$

Where:

$K_1 = 607{,}76\,Wm^{-2}sr^{-1}\mu m^{-1}$ e $K_2 = 1260{,}56\,K$

with K_1= 607,8 and K_2 = 1261 are in *mW/cm²/sr/µm*, they are constants used for the sensor Landsat 5 - TM (Allen et al., 2002).

The long-wave radiation, obtained by the Stefan-Boltzmann equation:

$$R_{L\uparrow} = \varepsilon_0 . \sigma . T_s^4 \ (Wm^{-2})$$

where ε_0 is the surface emissivity card, σ is the Stefan-Boltzmann constant ($\sigma = 5{,}67 \times 10^{-8}\ Wm^{-2}K^{-4}$) e T_s is the surface temperature (K) obtained in the previous step.

Short Wave Radiation Descending, obtained by the following expression:

$$R_{s\downarrow} = S . \cos Z . d_r . \tau_{sw}$$

where *S* is the solar constant (1367 Wm^{-2}, *Z* is the solar zenith angle, d_r is the inverse square of relative distance Earth-Sun (for both images the approximate value were 1.03.) and τ_{sw} is the atmospheric transmittance.

Calculate the outgoing long wave radiation incident by the following:

$$R_{L\downarrow} = \varepsilon_a . \sigma . T_a^4 \ (Wm^{-2})$$

Where ε_a is the emissivity of the atmosphere (dimensionless), σ is the Stefan-Boltzmann constant ($\sigma = 5{,}67.10^{-8}\ Wm^{-2}K^{-4}$), T_a air temperature (K) with ε_a represented by the following formula:

$$\varepsilon_a = 0{,}85.(-\ln\tau_{sw})^{0{,}09}$$

where τ_{sw} is the atmospheric transmittance.

Finally, it is determined the radiation balance (*Rn*) by the following expression:

$$Rn = R_{s\downarrow} + \alpha R_{s\downarrow} + R_{L\downarrow} - R_{L\uparrow} - (1 - \varepsilon_o) R_{L\downarrow}$$

where $R_{s\downarrow}$ is the short-wave radiation incident, α is the albedo, $R_{L\downarrow}$ is the long-wave radiation emitted by the atmosphere,, $R_{L\uparrow}$ is the long-wave

radiation emitted by the surface and ε_o is the emissivity of the surface.

Energy balance, the latent heat flux (*LE*) is provided by subtracting the flow of heat into the ground (*G*) and sensible heat flux (H) of the net radiation (*Rn*) by SEBAL (Bastiaanssen et al., 1998a; Jia et al, 2013):

$$LE = Rn - G - H \quad (\mathrm{Wm^{-2}})$$

The value of *G* is computed according to the empirical equation developed by Bastiaanssen (2000):

$$G = [\frac{Ts}{\alpha}(0{,}0038\alpha + 0{,}0074\alpha^2)(1 - 0{,}98IVDN^4)]\mathrm{Rn}$$

where *Ts* is the surface temperature (ºC), α is the surface albedo, NDVI is the normalized difference vegetation index and Rn is the surface net radiation.

The sensible heat flux was calculated from the equation proposed by SEBAL model:

$$H = \rho . c_p . dT / r_{ah}$$

where ρ is the air density $(1{,}15\,\mathrm{kgm^{-3}})$, c_p is the specific heat of the air $(1004\,\mathrm{Jkg^{-1}K^{-1}})$, dT (K) is the difference of temperature $(T_1 - T_2)$ between the two heights z_1 e z_2 and r_{ah} is the aerodynamic resistance to heat transport $(\mathrm{sm^{-1}})$.

3. Results and discussion

Methodologies for remote sensing used, the SEBAL to calculate H and LE flows, Allen (2002) for Rn and Bastiaanssen (2000) for G; plotted to scatter plots, and linear regressions referring to the days 24/10/2005 (Year of the Order of the Day - DOY 297) of the dry season and 08/08/2006 (DOY 220) the transition period (rainy to dry). From clippings of an area with banana orchard coverage, savanna vegetation and bare soil, compared the H + LE and Rn-G energy balance components, Figure 4.

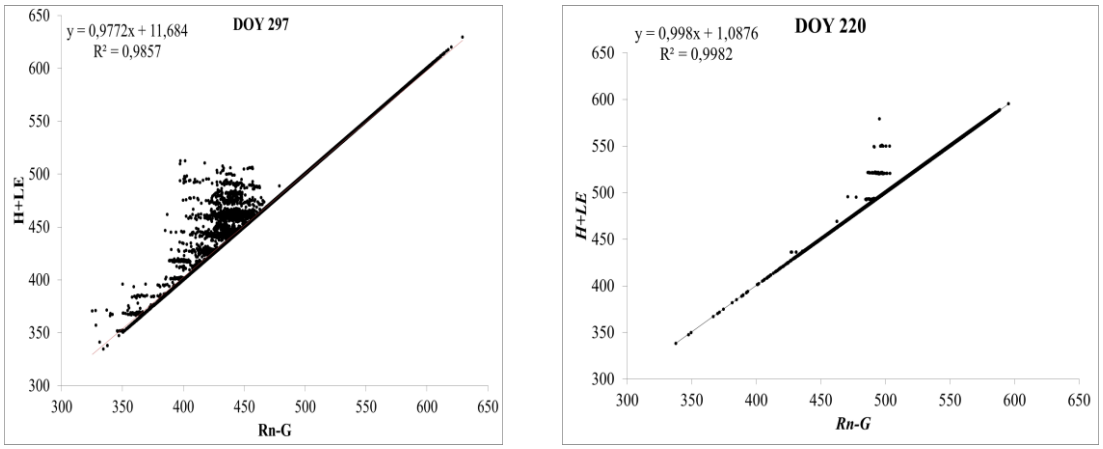

a) b)

Figura 4 - Scatter plot and coefficient of determination (R^2) of two days, DOY 297 (a) and DOY 220 (b).

It can be seen in Figure 4 that both dispersions showed quite satisfactory correlation between the quantities compared with correlation (r) greater than or equal to 0.99 and less than 2% of unexplained variance.

From a fragment of a banana orchard area, determined the relations of linear regression and were extracted scatter charts, of the two days (297 and 220) using the surface albedo and radiation balance (Rn), in Figure 5. The explained variation remained higher than 78%, that is, with higher correlations than 0.88, indicating that there is a strong relationship between the variables.

Based on the same approach taken by Borges et al. (2013) compared the variation of Rn with the surface albedo, to DOY 297, the dry season, and DOY 220, transition period, as shown in Figure 6.

By definition Varejao-Silva (2006) the albedo is the fraction of global radiation that is reflected, so the albedo is higher the radiation released into the atmosphere will be too. It is noted that in Figure 6, both dates analyzed, and the albedo Rn exhibited opposite behavior, according expected.

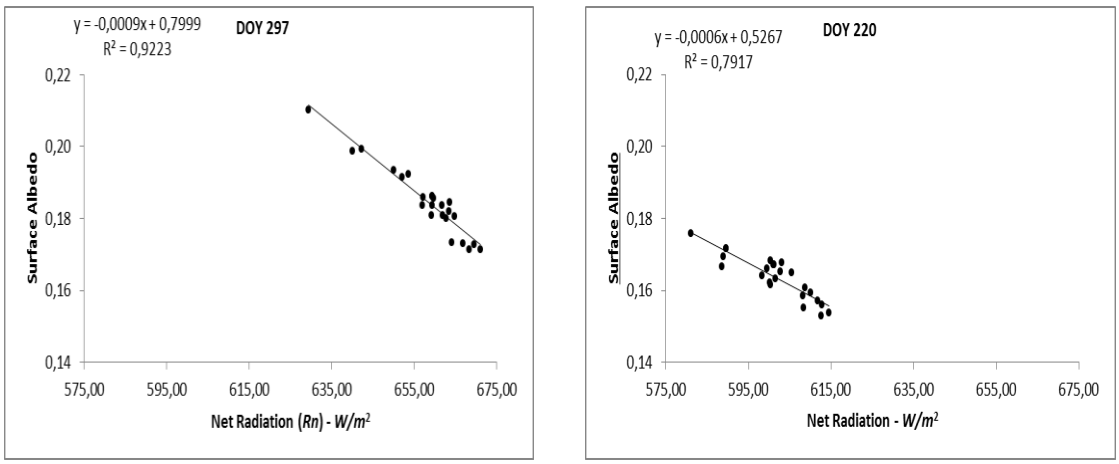

a) b)

Figura 5 - Correlations between the surface albedo and net radiation (Rn) to orchard area in days 297 (a) and 220 (b).

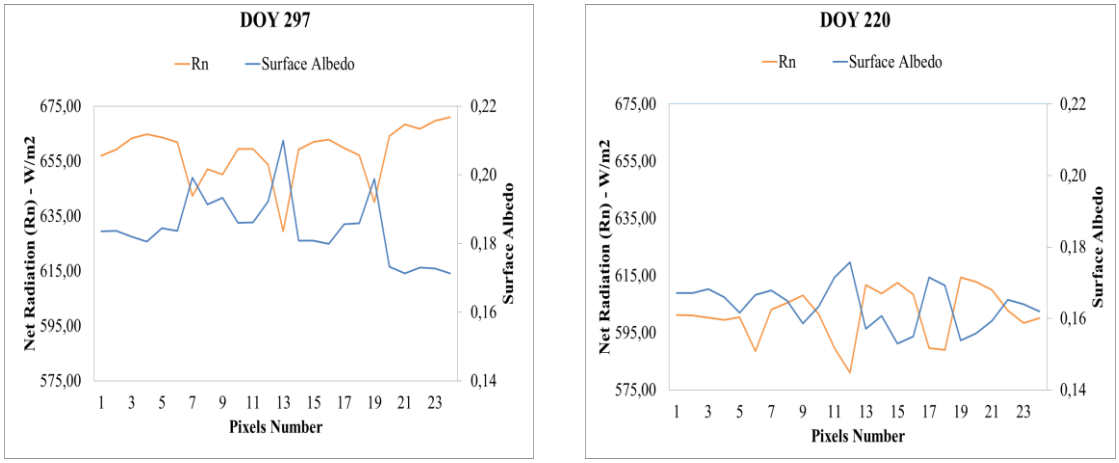

a) b)

Figura 6 - Comparison between the net radiation (Rn) with the albedo orchard area in days 297 and 220 (a, b).

From NDVI and surface temperature (Ts), made a comparison between them to an orchard's crop, Figure 7.

The NDVI may be used as a parameter indicator of the spatio-temporal dynamics of heterogeneous surfaces, as in the case of vegetation to water stress absorbing less solar radiation in the visible and increasing reflection (greater albedo), which enhances absorption in the infrared range producing lower NDVI and higher surface temperatures. Already the vegetation exhibits higher NDVI value, due to the high absorption of photosynthetic radiation in the red wavelength (Bezerra, et al, 2011;. 2014; Silva, 2009).

It may be noted in Figure 7 that the NDVI and Ts vary inversely in general, which is evident in Figure 7b, which is representative of the transition period where there is still water available in the soil.

In Figure 8 it can be seen that the day 297 did not show good correspondence between the variables analyzed, around 69% of unexplained variation. However, on day 220 was good correlation between Rn and albedo, as on this day the vegetation cover had possibly homogeneous characteristics; because of moisture available to be higher than on 297.

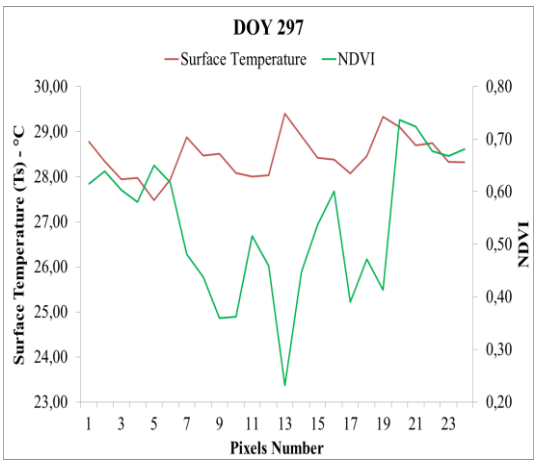

a)

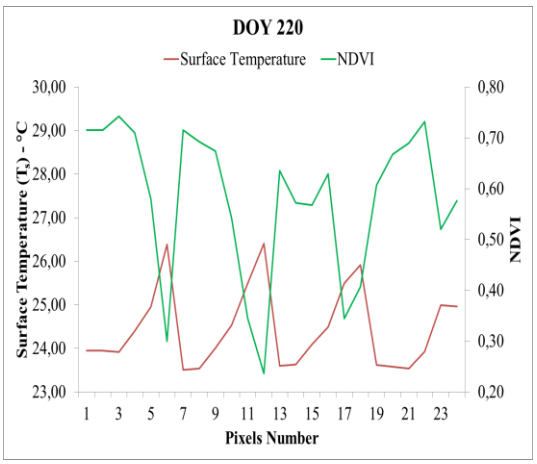

b)

Figura 7 - Comparison between the surface temperature (Ts) with NDVI to orchard area in days 297 and 220 (a, b).

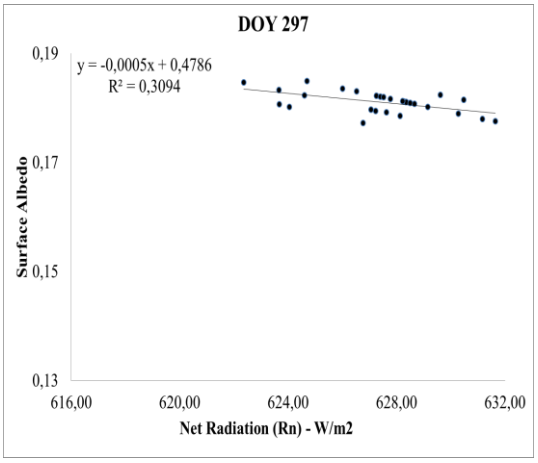

a)

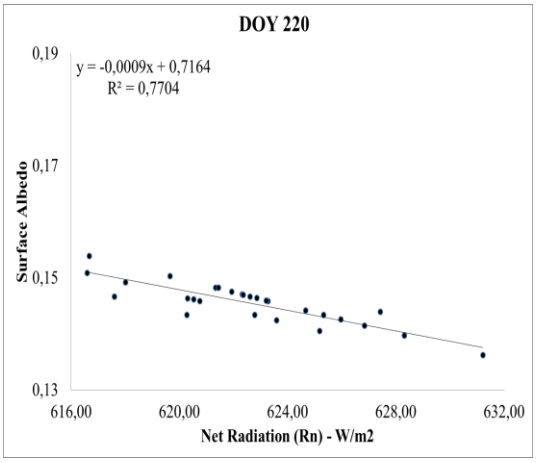

b)

Figura 8 - Correlations between the surface albedo and net radiation (Rn) to savanna area in days 297 (a) and 220 (b).

In the savanna area where the surface has heterogeneous characteristics, such as was commented on Bezerra et al. (2014), the albedo did not show much variation with respect to Rn (Figure 9a), corresponding to the dry season; it can be observed the sharpest contrast between the variables on day 220, Figure 9b.

In savanna area where the surface has heterogeneous characteristics, so there was no variation in the surface temperature, different from the more marked variation of NDVI mainly on 220 where the soil contains moisture (Figure 10).

From the surface clippings and albedo radiation balance was calculated linear regression for days 297 and 220, Figure 11a and 11b. Both dispersions showed coefficient greater than 0.90 determinations (r> 0.95), indicating a strong correlation between the variables, with less than 10% of unexplained variation.

In Figure 12, it can be clearly seen that for the bare soil, Rn and albedo vary inversely, that is, when Rn is high albedo is low and vice versa. Expected behavior for this type of surface, such as Bezerra et al. (2014) found high albedo values in these cases.

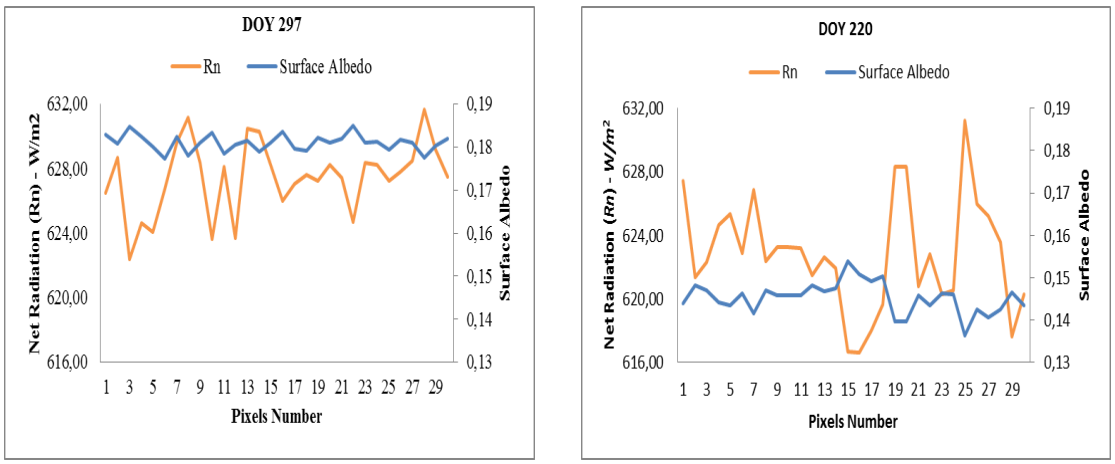

a) b)

Figura 9 - Comparison of net radiation (Rn) with the albedo to savanna area, on days 297 and 220 (a, b).

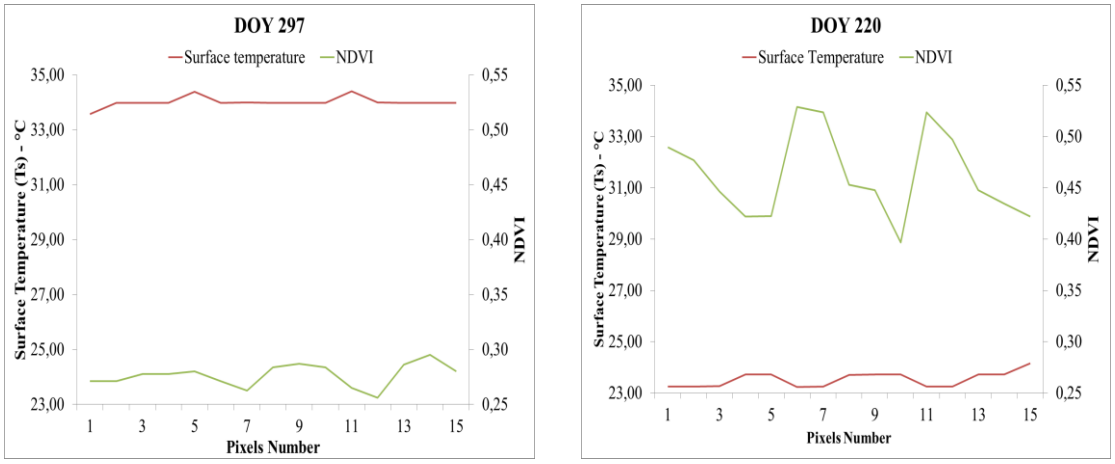

a) b)

Figura 10 - Comparison between the surface temperature (Ts) with NDVI, for savanna area in days 297 (a) and 220 (b).

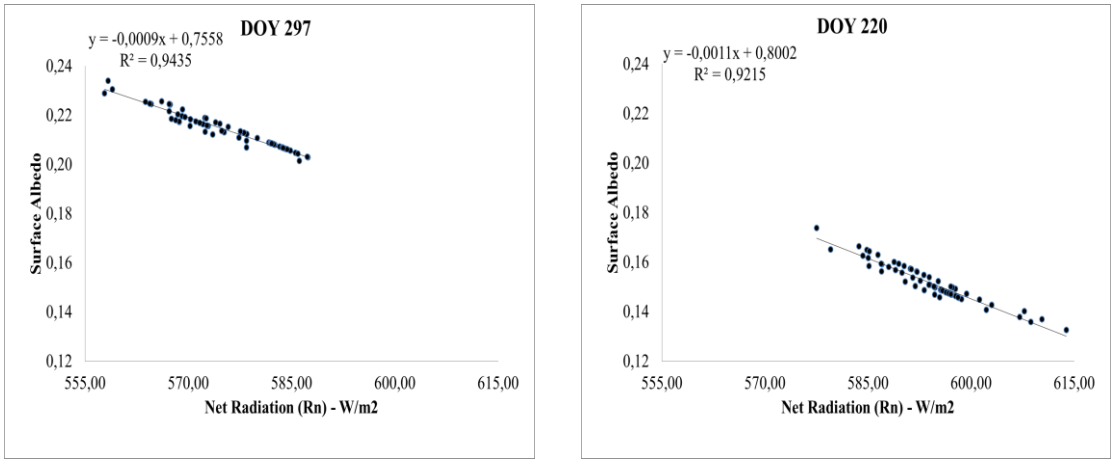

a) b)

Figura 11 - Correlations between the surface albedo and net radiation (Rn) for bare soil area, on days 297 (a) and 220 (b).

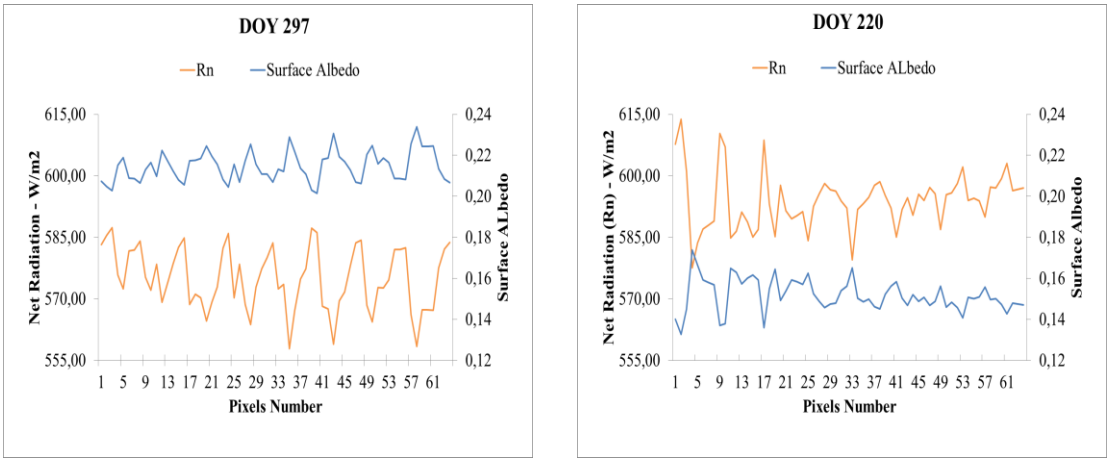

a) b)

Figura 12 - Comparison between the net radiation (Rn) with the albedo for the bare soil area, on days 297 (a) and 220 (b).

Analogously to that obtained for savanna, the surface temperature almost no variation for the bare soil (Figure 13), and the NDVI showed greater variation, especially on day 220 (Figure 13b).

Table 2 shows the averages of flows Rn, H, LE and albedo, for two studied days, 297 and 220, wherein the albedo exhibited values of approximately 0.2. Bezerra . et al. (2014) found for irrigated areas, values from 0.15 to 0.25, and for vegetated area by dense savanna in the dry season, values 0.15 to 0.20 due to the loss of shoots canopy leaf. On the bare soil, there were values between 0.25 to 0.30. According to Rodrigues et al. (2009), the albedo of 0.26 to 0.36 for bare soil, and savanna between 0.10-0.15.

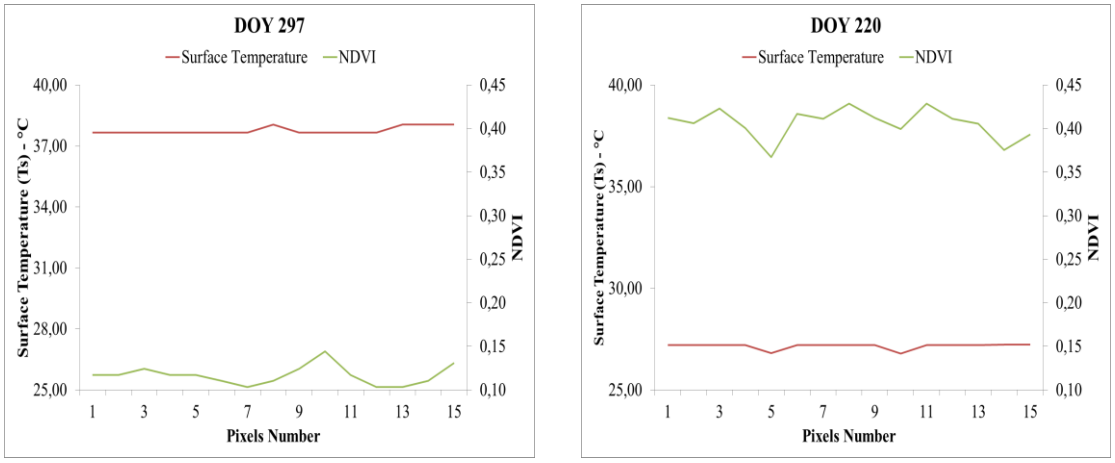

a) b)

Figura 13. Comparison of surface temperature (Ts) with NDVI for bare soil area, on days 297 (a) and 220 (b).

Rn flow (Table 2) was higher in agriculture, 629.9 W/m^2, the surface covered by savanna vegetation was 625.1 and the surface without vegetation cover 584.5. According to Leiva et al. (2007), *Rn* obtained was 662 to water, 585 to soil exposed, 606 to vegetated and 604 to urban area. Thus, the vegetated surfaces and bodies of water expected value greater *Rn* and less value for bare soil.

The *H* flux, Table 2 displays greater value to savanna, 287.5 $W/m^2$and the lowest for the orchard, 111.8 W/m^2. For *LE* (Table 2), in

W/m^2occurred values of 443.5 for the orchard, 230.6 to savanna, which was smaller than the above ground of 315.1. According to Santos (2009), the highest values of latent heat are in areas with lower vegetation cover (NDVI less than 0.4). It describes that occurred *LE* values (W/m^2) between -108 and 321 regions almost naked, also have the lowest values, between 624 and 778 representative of rice fields and water bodies.

Table 2 - Average values of sensible heat flux (*H*), latent (*LE*), net radiation (*Rn*) and albedo for different ground covers.

Soil Cover	*H* (W/m^2)	*LE* (W/m^2)	*Rn* (W/m^2)	*Albedo*
Orchard	111,8	443,5	629,9	0,2
Savanna	287,5	230,6	625,1	0,2
Bare Soil	171,9	315,1	584,5	0,2

The spatial variation of albedo and net radiation, displayed in Figure 14. In the areas with green and yellow colors (Figure 14 a, b) between the values of 0.10-0.20 which are corresponding to vegetated surfaces (savanna or agriculture). Albedo surfaces with greater than 0.25 are possibly of bare soil areas. In Figure 13b was the predominance of yellow and green, possibly related to the higher moisture content in the soil at this time (transition period for rainy to dry) than the previous. The radiation balance (Figure c, d) shows the highest values likely in vegetated areas, with green and yellow colors (550-650 W/m^2). The Rn with values between 400 and 550 W/m^2, corresponding to the gray, dark blue and light blue, indicating little or none vegetation. On 220 (transition period), Figure 14d, the variability of Rn was smaller than on 297, where the yellow and green highlighted.

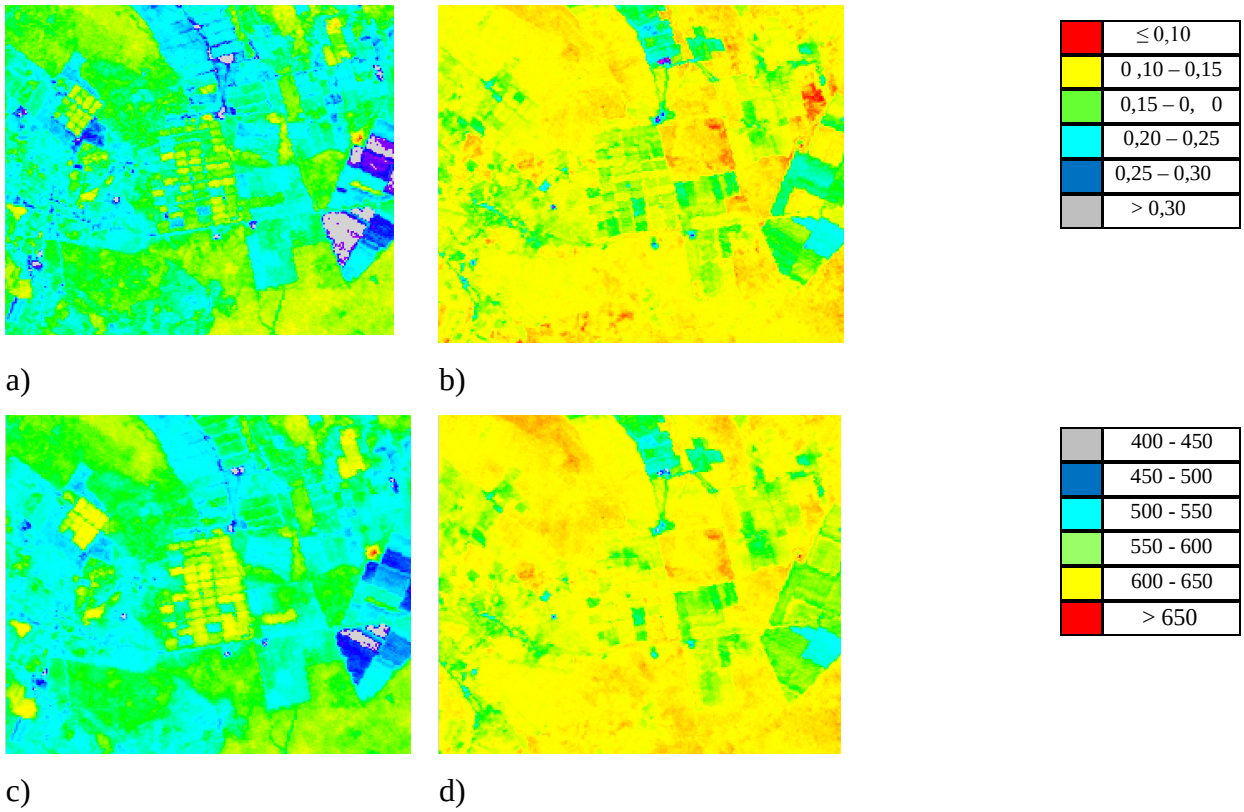

Figura 14 - Spatial distribution of the albedo for days 297/2005 (a) 220/2006 (b) Rn (W/m^2) for days 297/2005 (c) 220/2006 (d) and their respective palettes colors.

4. Conclusions

The qualitative analysis of biophysical parameters obtained by SEBAL showed the behavior and variability for different occupations and land use. The parameters estimated by the algorithm showed similar effects to those of other studies in the semiarid region with the literature cited.

Showing thus it is an important technique in remote sensing for monitoring the spatial variability of surface energy fluxes and biophysical parameters, in addition to complement or replace the analysis of observed data when absent.

References

Allen, R., Tasumi, M., Trezza, R., 2002. SEBAL - Surface Energy Balance Algorithms for Land – Advanced Training and User's Manual – Idaho Implementation, version 1.0.

Bastiaanssen, W.G.M., 2000. SEBAL. Based sensible and latent heat fluxes in the irrigated Gediz Basin, Turkey. Journal of Hidrology 229, 87-100.

Bastiaanssen, W.G.M., Menenti, M., Feddes, R.A., Holtslag, A.A.M., 1998a. A remote sensing surface energy balance algorithm for land (SEBAL) 1. Formulation. Journal of Hydrology 212-213, 198-212.

Bezerra, J.M., Moura, G.B.A., Silva, B.B., Lopes, P.M.O., Silva, E.F.F., 2014. Parâmetros biofísicos obtidos por sensoriamento remoto em região semiárida do estado do Rio Grande do Norte, Brasil. Revista Brasileira de Engenharia Agrícola e Ambiental 18, 73-84.

Bezerra, M.V.C., Silva, B.B.da, Bezerra, B.B., 2011. Avaliação dos efeitos atmosféricos no albedo e NDVI obtidos com imagens de satélite. Revista Brasileira de Engenharia Agrícola e Ambiental 15, 709-717.

Borges, C.K., 2013. Obtenção da evapotranspiração real diária através da aplicação de técnicas de sensoriamento remoto no semiárido brasileiro. Thesis (Master). Campina Grande, UFCG.

Borges, C.K., Santos, C.A.C., Medeiros, R.M., 2013. Análise qualitativa da evapotranspiração horária e sua comparação com o saldo de radiação. Revista Ciência e Natura, edição esp., 75-77.

Cunha, J.E.B.L., Rufino, I.A.A., Silva, B.B., Chaves, I.B., 2012. Dinâmica da cobertura vegetal para a Bacia de São João do Rio do Peixe, PB, utilizando-se sensoriamento remoto. Revista Brasileira de Engenharia Agrícola e Ambiental 16, 539-548.

Dantas, F.R.C., Braga, C.C., Souza, E.P., Silva, S.T.A., 2010. Determinação do albedo da superfície a partir de dados AVHRR/NOAA e TM/LANDSAT-5. Revista Brasileira de Meteorologia 25, 24-31.

Gómez, C., White, J.C., Wulder, M.A., 2011. Characterizing the state and processes of change in a dynamic forest environment using hierarchical spatio-temporal segmentation. Remote Sensing of Environment 115, 1665-1679.

Jia, D., Kaishan, S., Zongming, W., Bai, Z., Dianwei, L., 2013. Evapotranspiration Estimation Based on MODIS Products and SurfaceEnergy Balance Algorithms for Land (SEBAL) Model in Sanjiang Plain,Northeast China. Science 23, 73–91.

Leivas, J., Gusso, A., Fontana, D. C., Berlato, M., 2007. Estimativa do balanço de radiação na superfície a partir de imagens do satélite ASTER. XIII Simpósio Brasileiro de Sensoriamento Remoto, 255-262.

Lima, E.P., 2013. Estimativa da evapotranspiração real diária em sub-bacias do Paracatu utilizando produtos do sensor MODIS, in: Silva, B.B. (Org.). Aplicações Ambientais Brasileiras com Geoprocessamento e Sensoriamento Remoto. EDUFCG, Campina Grande, pp. 48.

Rodrigues, J.O., Andrade, E., Teixeira, A.S., Silva, B.B., 2009. Sazonalidade de variáveis biofísicas em regiões semiáridas pelo emprego do sensoriamento remoto. Revista Brasileira de Engenharia Agrícola e Ambiental 29, 452-465.

Sampaio, M.S., Alves, M.C., Carvalho, L.G., Sanches, L., 2011. Uso de Sistema de Informação Geográfica para comparar a classificação climática de Koppen-Geiger e de Thornthwaite. XV Simpósio Brasileiro de Sensoriamento Remoto, 8858.

Santos, C.A.C., 2009. Estimativa da evapotranspiração real diária através de análises micrometeorológicas e de

sensoriamento remoto. Thesis (Doctoral). Campina Grande, UFCG.

Santos, C.A.C., Silva, B.B., 2008. Estimativa da evapotranspiração da bananeira em região semiárida através do algoritmo S-SEBI. Revista Brasileira de Agrometeorologia 16, 9-20.

Santos, C.A.C., 2011. Análise das necessidades hídricas da vegetação tamarisk através da razão de Bowen e do modelo SEBAL. Revista Brasileira de Meteorologia 2685-94.

Santos, T.V., 2009. Fluxos de calor na superfície e evapotranspiração diária em áreas agrícolas e de vegetação nativa na bacia do Jacuí por meio de imagens orbitais. Thesis (Master). Porto Alegre, UFRGS.

Silva, S.T.A., 2009. Mapeamento da evapotranspiração na bacia hidrográfica do Baixo Jaguaribe usando técnicas de sensoriamento remoto. Thesis (Doctoral). Campina Grande, UFCG. 119.

Varejão-Silva, M.A., 2006. Meteorologia e Climatologia. Versão Digital 2.